



Synthesis of Fe₃O₄/ZnO nanoparticles and their application for the photodegradation of anionic and cationic dyes

O. Długosz¹ · K. Szostak¹ · M. Krupiński² · M. Banach¹

Received: 19 February 2020 / Revised: 31 May 2020 / Accepted: 14 July 2020 / Published online: 21 July 2020
© The Author(s) 2020

Abstract

Multifunctional materials have become an important research subject in recent years. Zinc oxide nanoparticles (ZnO NP) deposited on iron oxide (Fe₃O₄) allow to obtain material with photocatalytic and magnetic properties. The mass share of Fe₃O₄ in the composite was 30%. Saturation magnetization for this sample was about 9.5 emu/g. The use of magnetic material allows to recover the photocatalyst after the photodegradation process and reuse it. The possibility of recovery of Fe₃O₄ nanoparticles with a magnet was estimated at 94.80%, while the recovery of Fe₃O₄/ZnO achieved 83.91%. The effects of the type of dyes (Methylene Blue, Methyl Orange, Quinoline Yellow, Eriochromic Black T and Trypanic Blue) on their photodegradation efficiency in terms of molar mass of the dye, the solvent in which the processes were carried out and the type of dye charge were investigated. The photocatalytic material showed higher photodegradation activity of dyes while increasing their molar mass. ZnO NPs deposited on Fe₃O₄ presented 95.61% photocatalytic efficiency against Trypan Blue and 63.02% against Methylene Blue. Increasing the surface area of the catalyst to 39 m²/g and the presence of micro-, meso- and macropores had a positive effect on the sorption process of dyes, especially those of larger sizes, allowing their degradation in the photodegradation process.

Keywords Zinc oxide · Iron oxide · Magnetically separable photocatalyst · Nanoparticles · Microwave synthesis · Dyes

Introduction

Semiconductor metal oxides have been used widely in many fields of applications in electronics such as photocatalysis processes, adsorption of heavy metals, solar cells and gas sensors (Regulacio and Han 2016; Elilarassi and Chandrasekaran 2017). Zinc oxide nanoparticles (ZnO NPs) are an example of semiconductors widely used in many industrial and consumer products. One of the most characteristic properties of the ZnO NPs is photocatalytic activity (Riyadh et al. 2015; Fowsiya et al. 2016).

Combined with environmentally friendly properties and antimicrobial efficacy, ZnO NPs are very popular among scientists who study and their photocatalytic properties (Ghosh et al. 2019). Addition of zinc oxide metal and metal oxides can improve NPs photodegradation activity (Kant and Kumar 2012). There are a lot of studies which confirm higher photoactivity of modified ZnO compared to pure oxide or titanium oxide. Türkyılmaz et al. synthesized the ZnO modified by different noble and transition metals (Ni, Mn, Fe and Ag). They showed that the results of the photocatalytic degradation of tartrazine in aqueous solutions under the UV light confirmed that Ni/ZnO exhibited higher photocatalytic activity than the others (the maximum degradation of Tartrazine was 98.2% after 60 min of conduction). Depending on doped metal, photocatalytic activity generally could be higher than pure ZnO; however, the addition of manganese nanoparticles (Mn NPs) decreases the photocatalytic properties of modified ZnO (Türkyılmaz et al. 2017). Photocatalytic properties are also enhanced by metal oxide NPs (Atla et al. 2018; Güy et al. 2018; Andrade et al. 2019). In this case, the addition of metal oxide particles could have two functions. Firstly, compounds with different valences

Editorial responsibility: Gaurav Sharma.

✉ O. Długosz
odlugosz@chemia.pk.edu.pl

¹ Institute of Chemistry and Inorganic Technology, Cracow University of Technology, Warszawska St. 24, 31-155 Kraków, Poland

² Institute of Nuclear Physics, Polish Academy of Sciences, Kraków, Poland



can change the band gap in the whole product and improve the photoreduction processes. Secondly, a combination of two metal oxides can create uneven surfaces. Differences in the structures can be beneficial in creating vacancies and degraded surfaces which can be useful in electron transfers (Kansal et al. 2007; Goyal et al. 2018). Additionally, if ZnO NPs are synthesized on the surface of other metal oxide NPs, the metal oxide can change the porosity of the material. A higher degree of porosity improves adsorption of the compound on the surfaces of ZnO-based material. The high effectiveness of sorption of a compound is an important stage in photodegradation, because only after combination with a photocatalyst compound a good degree of decomposition can be guaranteed.

Modification of ZnO NPs by various metal and metal oxide NPs not only can improve the photocatalytic properties of ZnO NPs but also add brand-new properties, creating multifunctional products (Ahn et al. 2018; Sin et al. 2018). Examples of that are materials based on ZnO with Fe₃O₄ NPs, which present high photocatalytic activity with magnetic properties (Wang et al. 2016). This combination allows the creation of material for the photodegradation process in various solutions with easy and fast recovery of material after the process, by using a magnetic source (Elazab et al. 2017). A strong external magnetic field separates composite, which makes the separation easy, and without filtration stage. For the process to be effective, ZnO NPs have to be strongly associated with iron oxide NPs. There are some studies focused on the synthesis of Fe₃O₄/ZnO NPs. Fernández et al. synthesized a Fe₃O₄/ZnO nanocomposite. They synthesized Fe₃O₄ based on the Massart's method, whereas the Fe₃O₄/ZnO was prepared using polyol-mediated method. The nanocomposite proved effective for antibiotic removal (Fernández et al. 2019). Dehghan et al. obtained Fe₃O₄/ZnO-graphene oxide, which was active in visible light and significantly degraded metalaxyl (Dehghan et al. 2019).

In this paper, Fe₃O₄/ZnO NPs were synthesized with microwave irradiation to combine both the advantages of magnetic properties of Fe₃O₄ and photocatalytic properties of ZnO. Fe₃O₄ NPs were synthesized by the co-precipitation of Fe³⁺ and Fe²⁺. After the process, the ZnO NPs were synthesized onto the solid Fe₃O₄. The activity of the material was investigated for the degradation of a few solutions of dyes under UV light. The effects of the kind of the molar mass of dyes and type of the dyes were examined.

Materials and methods

Materials

Iron(II) sulphate (FeSO₄ · 7H₂O, Sigma-Aldrich), iron(III) chloride (FeCl₃ · 6H₂O, POCH) and zinc sulphate

(ZnSO₄ · 5H₂O, Sigma-Aldrich) were used to synthesize Fe₃O₄/ZnO NPs. Sodium carbonate (Na₂CO₃, Sigma-Aldrich) was used as a precipitating agent. Photodegradation processes of selected dyes were carried out to verify the photocatalytic properties of the material. Table 1 presents a list of the dyes used (Sigma-Aldrich) with the formula and their properties. Calibration curves to determine the concentration of dyes in solution with a determination factor were prepared and added to the table.

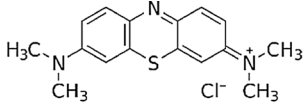
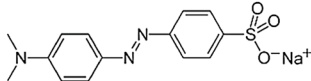
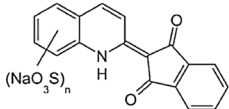
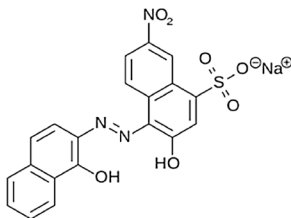
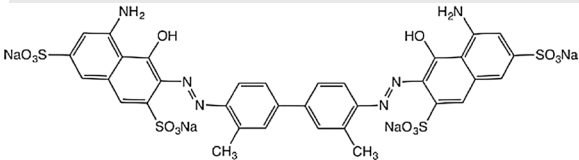
Preparation of Fe₃O₄/ZnO

Reactions were carried out in a microwave reactor (MAGNUM II, Ertec, Poland). Fe₃O₄/ZnO NPs were synthesized in a two-stage process. In the first stage, Fe₃O₄ NPs were prepared by mixing, under ultrasound irradiation, 10 cm³ of 1 M FeSO₄, 10 cm³ of 1 M FeCl₃ and then dropping of 12 cm³ of NaOH to get a pH of 9 in the solution. After 3 min, the suspension was transferred to a Teflon vessel and it was heated in the microwave reactor for 15 min at 180 °C. The iron oxide NPs were filtered and dried at 105 °C for 24 h. In the next step, 0.7 g of solid Fe₃O₄ was mixed using ultrasound irradiation with 20 cm³ of 1 M ZnSO₄ and 10 cm³ of 2 M NaCO₃. After three minutes, the suspension was transferred to a Teflon vessel and heated in the microwave reactor for 15 min at 180 °C. The Fe₃O₄/ZnO NPs were filtered and dried at 105 °C for 24 h.

Instrumental analysis

The magnetic and photocatalytic properties of Fe₃O₄/ZnO NPs were analysed. The surface of the material was investigated by transmission electron microscopy (TEM) with energy-dispersive X-ray analysis (EDX) using a Tecnai Transmission Electron Microscope (F20 X-Twin, FEI Europe). Confirmation of material structure with mass ratio of compounds was calculated on the base of X-ray powder diffraction (XRD) analysis (with a Philips X'Pert camera with monochromator PW 1752/00 CuKα). The Fourier Transform Infrared Spectroscopy (FTIR) (with Nicolet 380 spectrometer) method was used for confirmation of effectiveness of dyes sorption onto synthesized material. BET analysis carried out with Micromeritics USA model ASAP2010 was used in evaluation of the size of the pores and specific surface area of the Fe₃O₄/ZnO NPs (Abdel-Wahab et al. 2016). The magnetic properties of pure Fe₃O₄ and Fe₃O₄/ZnO before and after photodegradation were analysed in a temperature of 300 K. All measurements were carried out in the magnetic field range –70 to 70 kOe (corresponding to the range –7 to 7 T) using a SQUID magnetometer. Magnetic hysteresis of each material was conducted. Concentration of each dye was measured with the use of UV-Vis spectrophotometer (Rayleigh UV-1800) (Table 1).

Table 1 Dyes used in photocatalytic studies on Fe₃O₄/ZnO NPs

Formula	Molar mass [g/mol]	Character of the dye	Max Abs [nm]	Calibration Curve
Methylene Blue				
	319.9	Cationic	664	$R^2 = 0.9947$ $y = 0.1921x + 0.0244$
Methyl Orange				
	327.3	Anionic	464	$R^2 = 0.9998$ $y = 0.0735x + 0.0168$
Quinoline Yellow				
	477.4	Neutral	412	$R^2 = 0.9920$ $y = 0.0725x + 0.0792$
Eriochrome Black T				
	461.4	Anionic	534	$R^2 = 0.9985$ $y = 0.012x + 0.0505$
Trypan Blue				
	960.8	Anionic	590	$R^2 = 0.9970$ $y = 0.0353x + 0.0124$

The photocatalytic properties of materials were determined from the results of band gap values using UV–Vis spectroscopy (Rayleigh UV-1800 spectrophotometer). The values of the band gap were equal to the energy difference between the top of the valence band and the bottom of the conduction:

$$E_g = \frac{h \cdot c \cdot 10^{19}}{\lambda \cdot 1.6} [\text{eV}] \quad (1)$$

where h is Planck's constant = $6.626 \cdot 10^{-34} \text{ J} \cdot \text{s}$, c speed of light = $3.0 \cdot 10^8 \text{ m/s}$, λ cut off wavelength/absorption edge in nanometers band (Morales et al. 2007).

Photocatalytic degradation experiments

Photodegradation of each dye was carried out for 60 min, using 0.5 g of the material and 200 cm³ of dye solutions with different initial concentration, depending on the dye

type. The dye solution with the material was mixed using a mechanical stirrer, initially for 30 min in the dark, and then for 60 min under UV light at 365 nm. The efficiency of photocatalytic degradation of each dye was calculated on the base of the equation:

$$E = \frac{(C_0 - C_t)}{C_0} \cdot 100[\%] \quad (2)$$

The amount of the degraded dye R_D (mg/g) was calculated from the following equation:

$$R = \frac{(C_0 - C_t) \cdot V}{m} \left[\frac{\text{mg}}{\text{g}} \right] \quad (3)$$

where C_0 is the initial concentration (mg/dm³), C_t is the concentration of the dye solution after t minutes (mg/dm³), V is the solution volume (dm³), and m is the mass of the material (g).



Kinetic studies of Fe₃O₄/ZnO NPs

The rate of photodegradation for each dye was determined by the Langmuir–Hinshelwood kinetic model (L–H model) (Lee et al. 2015). The L–H model was used to investigate the heterogeneous photodegradation processes. The reaction rate (r) is represented by the equation:

$$r = \frac{K_1 K_2 C}{1 + K_2 C} \quad (4)$$

where K_1 and K_2 are the rate constant and the adsorption constant. After assuming that the dye concentration is low ($K_2 C \ll 1$) the reaction rate is transformed into a first-order equation (Patil et al. 2016). Based on the equation, the proportional coefficient, called the photodegradation rate constant (k [min^{-1}]), is as follows:

$$-\ln \frac{C}{C_0} = kt \quad (5)$$

Efficiency of dye photodegradation in subsequent cycles

Photocatalytic stability and the efficiency of reused Fe₃O₄/ZnO were evaluated. For this purpose, 0.6 g of catalyst was added to the dye solution ($C_0 = 100 \text{ mg/dm}^3$) and the concentration of the Trypan Blue was investigated by UV–Vis spectroscopic measurements for 30 min in darkness and 30 min under UV light. After measurement, the catalyst was separated from the solution by filtration and, without washing, it was dried at 100 °C. The dried catalyst was added into a new ($C_0 = 100 \text{ mg/dm}^3$) solution of the dye to reuse it for photocatalysis experiments. After each experiment, the dried catalyst was analysed by FTIR analysis to investigate differences in the structure of the catalyst.

Results and discussion

Effect of mass ratio of FeO, Fe₂O₃ and ZnO NPs on magnetic and photocatalytic properties of the material

In order to prevent agglomeration of photocatalyst in dyes solution, the authors used the microwave reactor as a reaction system. According to Alqadami et al., iron oxide magnetic nanoparticles often agglomerate. To avoid this phenomenon, they used citric acid or trisodium citrate to functionalize the surface of these nanoparticles (Alqadami et al. 2017).

In the following study, it was confirmed that the main factor affecting both photocatalytic and magnetic properties was the pH of the initial solution in which iron oxide NPs were obtained. The pH directly affects the proportion of the both synthesized iron oxides: Fe₂O₃, which enhanced the photocatalytic properties of the material, and FeO, which with Fe₂O₃ creates a magnetite phase Fe₃O₄, influencing the magnetic properties of the material. A series of tests were conducted in which iron oxide was obtained at different pH. Depending on the pH of the solution, various iron oxides were obtained, with a different proportion of Fe₂O₃ to FeO (Fe-6, Fe-8 and Fe-10, respectively). In the second stage, ZnO was synthesized on the surface of iron oxides and marked as: Zn–Fe-6, Zn–Fe-8 and Zn–Fe-10 composites. The materials were tested for their photocatalytic properties by determining their degree of Trypan Blue removal in mg/g. The results of the measurements are shown in Fig. 1.

The increase in the pH during the synthesis of iron oxide nanoparticles caused an increase in the FeO content, which improved the magnetic properties of the material. The iron oxide obtained at pH 6 contained mainly the Fe₂O₃ phase, which affected ZnO photocatalytic properties. However, the material did not purchase magnetic properties. The improvement in properties occurred as a result of the increased in the electron activity of ZnO. Abbas et al. confirmed that the addition of Fe₂O₃ to TiO₂ favourably changed the crystal structure of the material. The addition of 8% increased the sorption capacity of the material by 29%, at the same time enhancing the total photocatalytic performance of the material (Abbas et al. 2016). Hernández et al. studied the efficiency of cyanide degradation using ZnO–Fe₂O₃. The material obtained at pH 7 presented higher photocatalytic activity compared to the material obtained at pH 9. The authors confirmed that the higher iron content in composite reduced the distance that separated photoelectrons from the

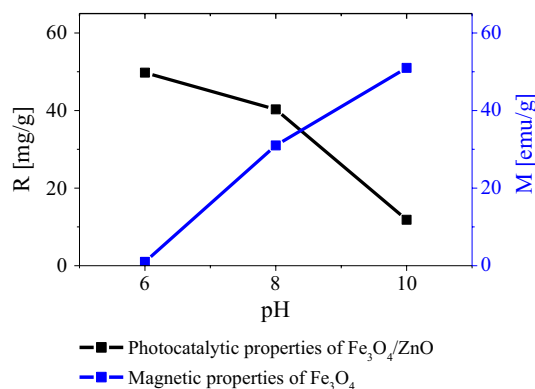


Fig. 1 Degree of Trypan Blue dye removal by ZnO deposited onto iron oxides and magnetic properties of iron oxides depending on the pH of the reaction for obtaining iron oxide

holes, which reflected the decrease in the activity of solids in the photocatalytic process (Hernández et al. 2007). The synthesis of iron oxide at pH 10 resulted in the absence of the Fe_2O_3 phase, replacing it with the magnetite Fe_3O_4 phase. The Fe_3O_4 material did not improve the sorption capacity, what was connected with decrease in Zn–Fe-10 photocatalytic activity.

The XRD analyses (Fig. 2) were carried out for iron oxides synthesized in different pH conditions, pure ZnO and the photocatalytic material (ZnO-Fe-8). The XRD plot of the pure-ZnO sample contained peaks at 2θ of 31.75, 34.35, 36.25, 47.50 and 56.60, which correspond to (100), (002), (101), (102) and (110), respectively, and were consistent with the hexagonal zincite structure of ZnO (Naqvi et al. 2014; Garino et al. 2019). The sharp and narrow shape of those peaks indicated the high crystallinity of the zinc oxide. The XRD pattern of iron oxide samples also showed that the material had good crystallinity. Peaks at 2θ of 30.20, 35.60, 43.20, 54.00 and 57.35 corresponding to (220), (311), (400), (422) and (511), were in the accordance with Fe_3O_4 structures (Bertolucci et al. 2015). The peaks at 2θ of 24.10, 33.10, 40.80 and 50.15 corresponded to (012), (104), (440) and (024) and were characteristic for the Fe_2O_3 phase (Aliahmad and Nasiri Moghaddam 2013; Han et al. 2014). All the above-mentioned peaks were present in the results of XRD analysis of the $\text{Fe}_3\text{O}_4/\text{ZnO}$ sample, which proved that both ZnO and Fe_3O_4 were present in the final material. The samples differed in terms of Fe_2O_3 and Fe_3O_4 content. Iron oxide samples synthesized at pH 6 (Fe-6) contained

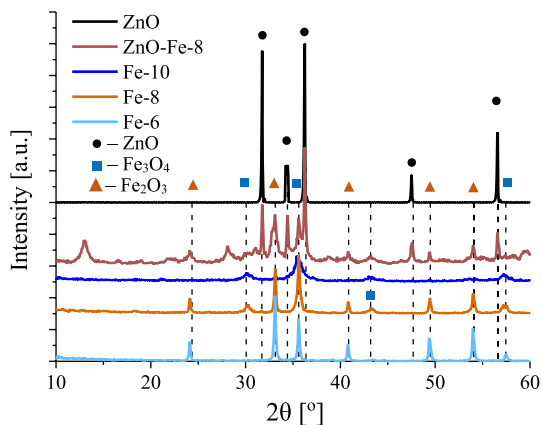


Fig. 2 XRD patterns of ZnO and iron oxide NPs synthesized in different pHs (Fe-6, Fe-8, Fe-10) and nanocomposites of $\text{Fe}_3\text{O}_4/\text{ZnO}$ (Zn–Fe-8)

Table 2 Band-gap values of the pure ZnO and $\text{Fe}_3\text{O}_4/\text{ZnO}$ NPs and magnetic material recovery of Fe_3O_4 and $\text{Fe}_3\text{O}_4/\text{ZnO}$

Properties of the materials	ZnO	Fe_3O_4	$\text{Fe}_3\text{O}_4/\text{ZnO}$
Band gap (eV)	3.18 ± 0.02	–	3.16 ± 0.02
Material recovery using a magnet (%)	–	94.80 ± 0.39	83.91 ± 1.31

94.6%_{wt} of Fe_2O_3 and 5.4%_{wt} of Fe_3O_4 . In contrast, iron oxide obtained at 10 pH consisted of 5.3%_{wt} of Fe_2O_3 and 94.7%_{wt} of Fe_3O_4 . Iron oxide, which was synthesized at 8 pH and used to obtain composition with ZnO, contained 28.0%_{wt} of Fe_2O_3 and 72.0%_{wt} of Fe_3O_4 . The final sample of Zn–Fe-8 consisted of 64.2%_{wt} ZnO, 9.3%_{wt} of Fe_3O_4 and 26.5%_{wt} of Fe_2O_3 .

Characterization

The characteristics of $\text{Fe}_3\text{O}_4/\text{ZnO}$ before and after photocatalytic processes with band gap and material recovery efficiency were examined (Table 2). The addition of iron oxide reduced the width of the energy gap, improving its photocatalytic activity, as confirmed in studies (Fig. 1). Additionally, by using a magnet applied to a vessel with a dispersed $\text{Fe}_3\text{O}_4/\text{ZnO}$, the possibility of separating the material from the liquid was checked.

Structure characteristics

Structural analysis confirmed the presence of nano-, micro- and macropores. The presence of both nano- and macropores significantly affected the sorption and subsequent decomposition of dyes. Depending on the dye structure and its molecular mass, different photocatalytic efficiency was observed. The material had a specific surface area of over 35.37 m^2/g (Table 3). The material after the photocatalytic process had a surface area 39.06 m^2/g . Such a difference might be due to the opening of closed pores during the photodegradation process and the removal of oxygen surface groups as a result of supply of energy in the form of ultraviolet radiation. Rodrigues et al. confirmed that thermal treatment can selectively remove some of the oxygen surface groups and thus slightly

Table 3 Specific surface areas, pore volume and pore surface of $\text{Fe}_3\text{O}_4/\text{ZnO}$ NPs before and after photodegradation process of Trypan Blue

Properties of the materials	$\text{Fe}_3\text{O}_4/\text{ZnO}$ before photodegradation	$\text{Fe}_3\text{O}_4/\text{ZnO}$ after photodegradation
Surface area (m^2/g)	35.37	36.06
Pore volume (m^3/g)	0.00072 (0.804 nm)	0.00072 (0.804 nm)
	0.1196 (86.25 nm)	0.1438 (93.13 nm)
Pore surface (m^2/g)	23.02 (0.804 nm)	25.91 (0.804 nm)
	8.256 (86.25)	9.564 (93.13 nm)



increase the active surface of the catalyst (Rodrigues et al. 2017).

ZnO deposited on iron oxide caused a small loss of the photocatalyst, which was due to a decrease in the magnetic properties of the composite, which is mentioned in Sect. 3.2.2. Sorption isotherm was II type with narrow hysteresis loops, which is characteristic of physical adsorption (Fig. 3). It is associated with the formation of a multi-molecular layer in which dye particles reach the occupied site of the bed, resulting in the formation of an intermediate adsorption complex.

TEM analysis showed the presence of different types of NPs in obtained material. Figure 4.1 shows the largest observed structures which are needle-shaped formations with a width of about 100–200 nm and a length of several micrometres. Irregular spherical nanoparticles with a size of 10–20 nm are deposited on the surface of ZnO NPs needles (Fig. 4.3). TEM analysis confirmed that the photocatalyst is stable and retains its original shape even after photocatalytic processes carried out with rapid mixing (Fig. 5).

Magnetic properties of Fe₃O₄/ZnO NPs

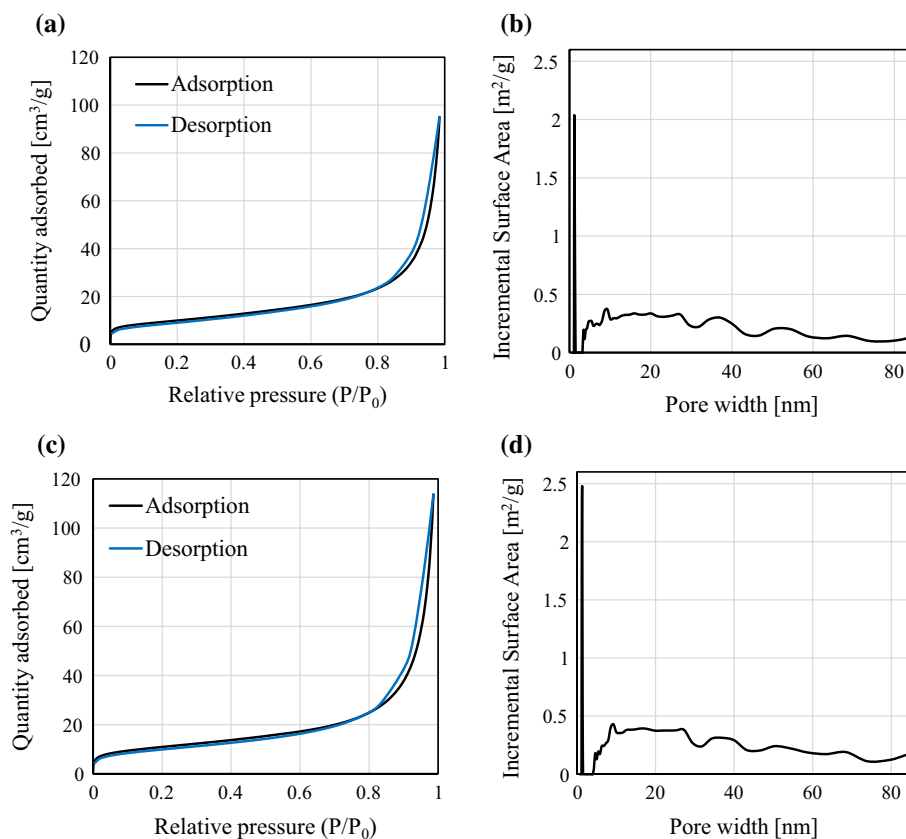
Hysteresis curves for Fe-6 and Fe-10 samples did not show any remanence or any coercive field (Fig. 6). The particles' magnetic moments were released at room temperature. The

particles could spontaneously change orientation, resulting in almost zero remanence and a negligible small force field, which was characteristic for superparamagnetic samples. In the case of the Fe-8 sample, nonzero remanence and there was a small coercive field of approximately 300 Oe. This might be due to the larger size of crystallites, which it meant that their moments of crystallites were also larger and did not reorient in the external field as easily as in the case of the Fe-6 and Fe-10 samples.

The values of the magnetization degree for the three samples were 1 emu/g (for the Fe-6 sample), 51 emu/g (for Fe-10) and 31 emu/g (for Fe-8). In each of these cases, the measured value was smaller than for solid magnetite (about 85 emu/g). The source of this difference can be seen mainly in the fact that the samples did not consist entirely of pure magnetite and contained admixtures of other iron oxides.

The properties of the Fe-10 sample were similar to the properties of nanoparticles, which included magnetite synthesized by chemical precipitation methods. The results of such measurements were presented in the works of Mieloch et al. (2018), Wierzbinski et al. (2018) and Kucharczyk et al. (2019). The magnetic nanoparticles consisted of about 70–80% of crystallized pure magnetite. For such systems at room temperature a similar shape and course of M (H) waveforms was obtained as in the Fe-10 sample. The saturation magnetization value was also similar and was

Fig. 3 BET Surface Area Plot with Incremental Surface Area for: **a, b** pure Fe₃O₄/ZnO NPs (Zn-Fe-8) and **c, d** Fe₃O₄/ZnO NPs after photodegradation of Trypan Blue



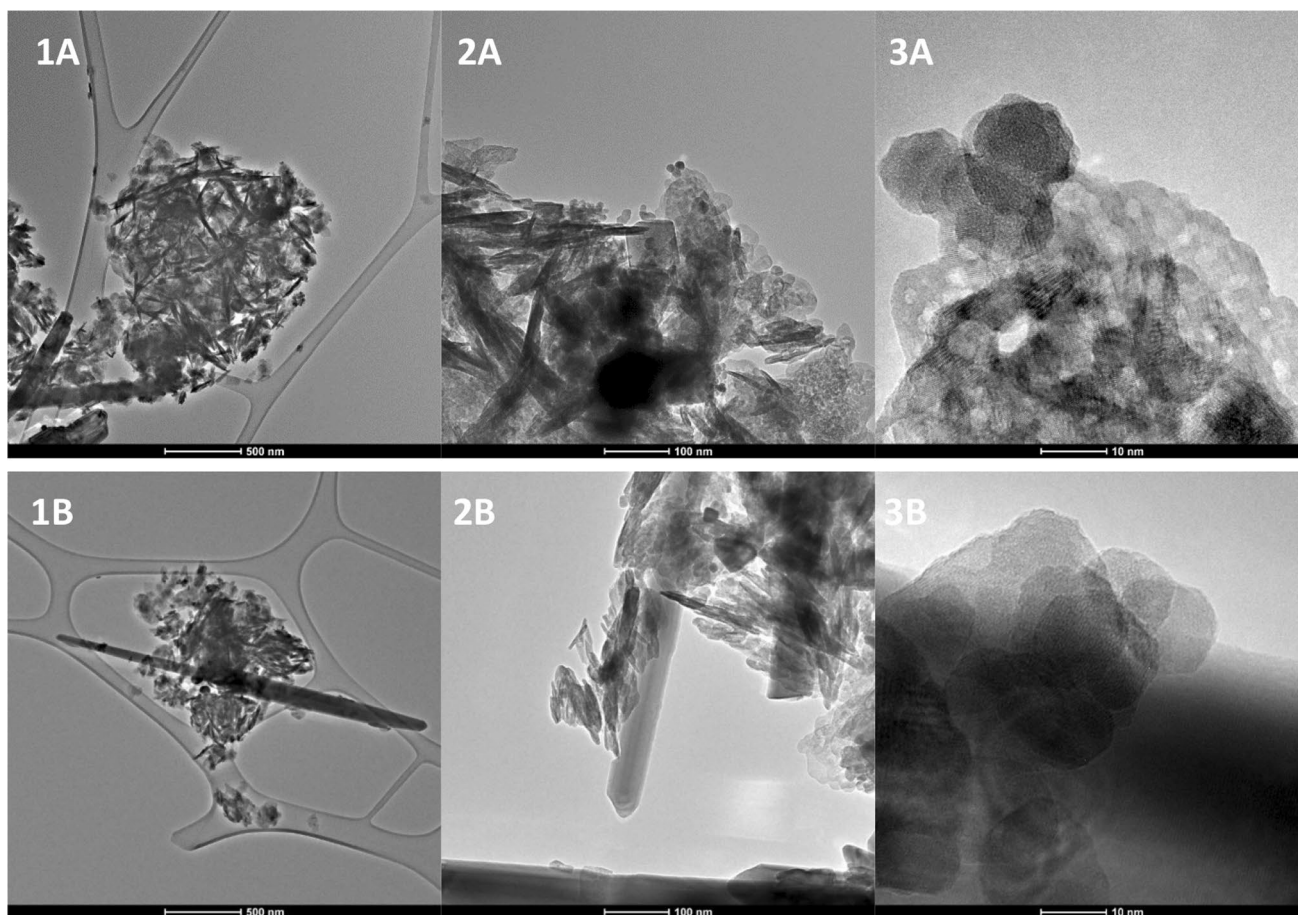


Fig. 4 TEM microphotographs of $\text{Fe}_3\text{O}_4/\text{ZnO}$ (Zn-Fe-8): A1-A3 before photocatalytic degradation of Trypan Blue, B1-B3 after photocatalytic degradation of Trypan Blue

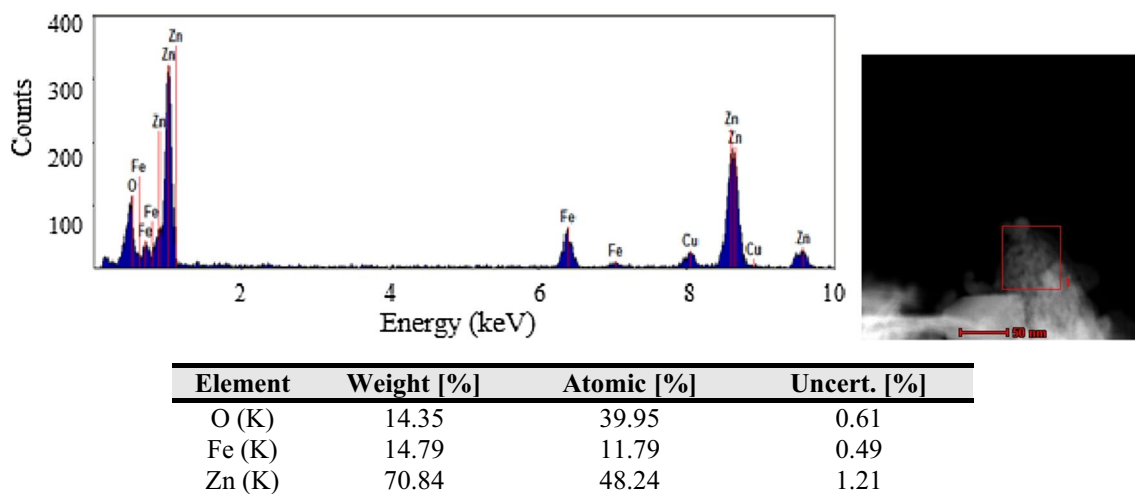


Fig. 5 TEM-EDX microphotographs of $\text{Fe}_3\text{O}_4/\text{ZnO}$ (Zn-Fe-8) before photocatalytic degradation of Trypan Blue

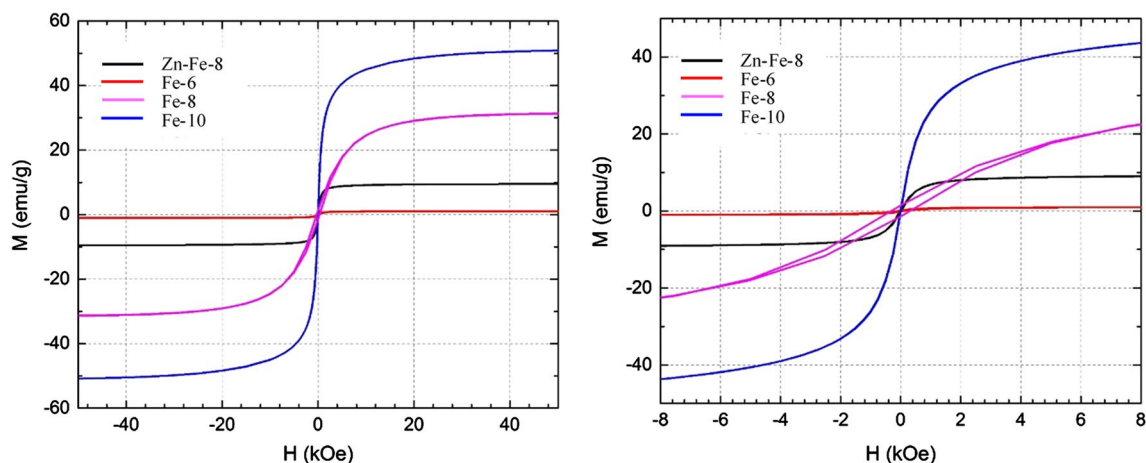


Fig. 6 Magnetic hysteresis loop of iron oxides (Fe-6, Fe-8, Fe-10) and ZnO NPs deposited on Fe_3O_4 (Zn-Fe-8)

about 60 emu/g. The Zn-Fe-8 sample, similar to the Fe-6 and Fe-10 samples, showed a negligible coercive field and a near-zero retention. It should be suspected that the magnetic phase contained in it consisted of superparamagnetic nanoparticles. Saturation magnetization for this sample was about 9.5 emu/g. Due to the fact that 30% of the samples were iron oxides, the magnetization of iron oxide saturation contained in the sample was about 31.5 emu/g. The results were consistent with the results of XRD analysis.

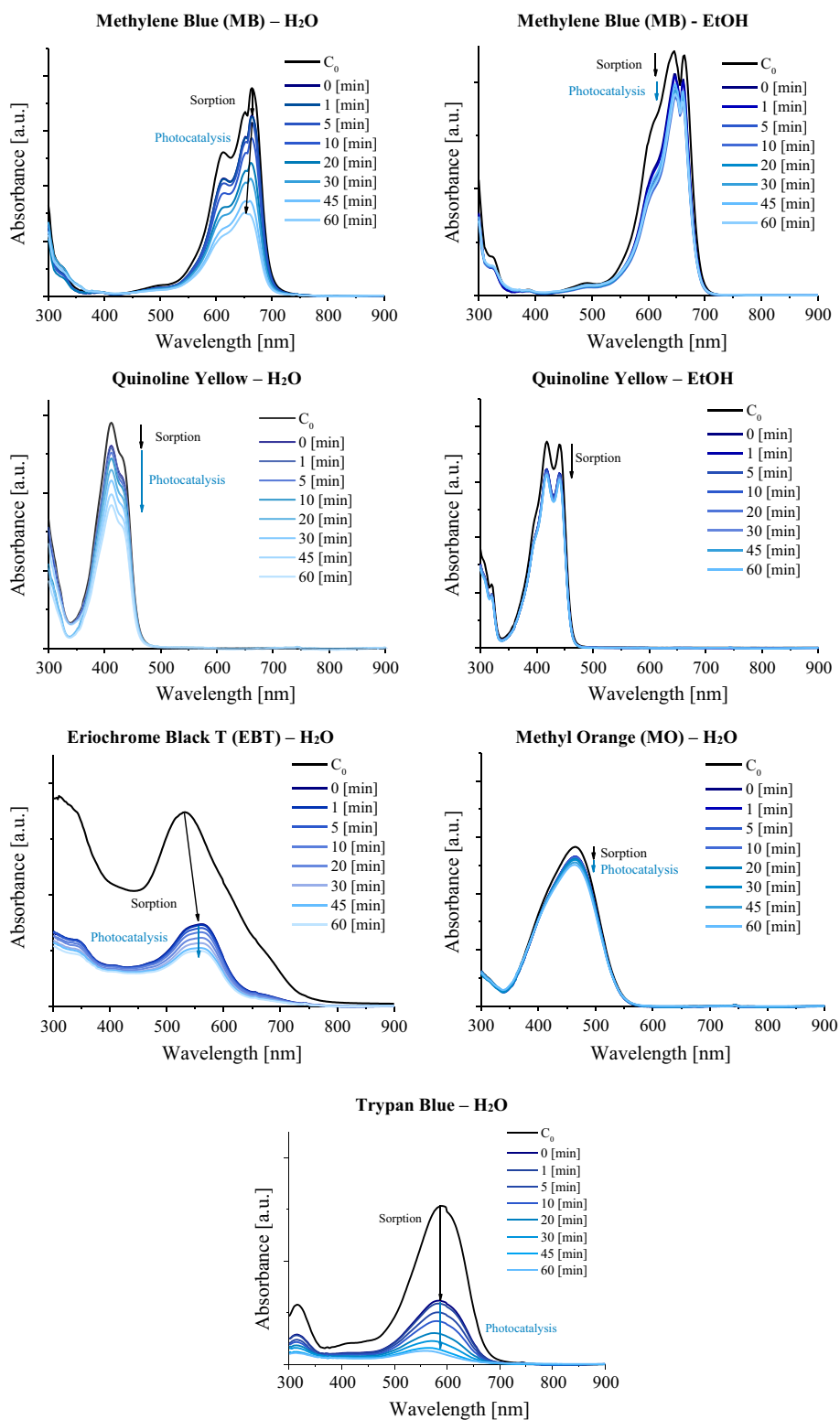
Photocatalytic degradation of dye solutions

Photocatalytic activity of the prepared material was influenced by surface properties of the catalyst, properties of adsorbed molecules, solvent used and parameters of the photodegradation process (temperature, system pH, etc.). Depending on the type of dye, a different degree of dye adsorption on the material as well as a different degree of photodegradation of dyes could be observed (Fig. 7). Methyl Orange was adsorbed in the lowest amount, which also affected the lowest degree of dye removal by photodegradation. This might be due to limited contact of the catalyst with the dye; therefore, the photocatalytic reactions were limited. By comparing the sorption process of Methylene Blue and Quinoline Yellow, a similar value of 13% dye reduction was obtained. When comparing reaction environments, the presence of hydroxyl groups was the key factor in photocatalytic processes (Table 4). Comparing the efficiency of the photodegradation process, significant influences of the solvent, dye particle size as well as the ionic nature of the dyes can be observed. It is worth to characterize individual systems taking into account more dye parameters. Due to this approach, it is possible to characterize the process in terms of its mechanism of reaction.

Effect of charge of dye

pH plays an important role in the sorption process and directly affects the process of photocatalysis. In this study it was decided to examine the effect of the charge of the dye itself at neutral pH and standard conditions. The photodegradation process was tested with the use of three dyes with different charges: Methylene Blue (MB) as a cationic dye, Quinoline Yellow (QY) as a neutral dye and Eriochrome Black T (EBT) as an anionic dye. The results are presented in the form of UV-Vis spectra in Fig. 7 and in Table 4. Taking into consideration the sorption process, it can be seen that MB and QY show a low degree of adsorption at about 13% and 11%, respectively, while the amount of adsorbed EBT reached almost 62%. The greater affinity of the anionic substance for the material under the process conditions indicated a positive surface charge of photocatalyst (Ben Arfi et al. 2017; Bel Hadjltaief et al. 2018). Comparing the quantities of dye adsorbed to the overall degree of dye removal after the photocatalysis process, it was observed that the high removal value after the sorption process did not condition high final result. Despite similar sorption efficiencies both for QY and MB, their photodegradation efficiency differed significantly—38.65% and 63.02% for QY and MB, respectively. A positive-charged dye can have a stronger affinity for the radicals formed in the presence of UV light, so that their photocatalytic degradation will take place at a higher rate. It is assumed that a negative charge that favours the sorption process may limit the photodegradation process. However, the process is not yet fully understood and therefore requires further research.

Fig. 7 UV-VIS spectrum of dye solution during 1 h photocatalytic processes on $\text{Fe}_3\text{O}_4/\text{ZnO}$ (Zn-Fe-8) NPs



Effect of molar mass of dye

According to the results of surface analysis, it can be expected that due to the presence of all three types of pores, i.e., micro (< 2 nm), meso (2–50 nm) and macro (> 50 nm),

a wide spectrum of molecules should be able to adsorb onto the surface of the tested material. Three dyes with different molar mass were selected in order to examine their possible influence on the degradation process: Methylene Blue (MB)—319.9 g/mol, Eriochrome Black T (EBT)—461.4 g/



Table 4 Photodegradation efficiency of each dye onto Fe₃O₄/ZnO (Zn-Fe-8) NPs

Dye	Solvent	C ₀ (mg/dm ³)	Sorption (min)		Photodegradation (after 30 min in darkness) (min)					
			30	1	1	5	10	20	30	45
Methylene Blue	H ₂ O	20	13.23	14.03	16.81	24.42	36.73	44.76	56.17	63.02
Methylene Blue	EtOH	20	13.22	14.51	19.22	24.96	22.56	22.25	19.00	24.30
Methyl Orange	H ₂ O	20	6.22	6.22	6.37	6.65	7.58	8.22	9.87	11.37
Quinoline Yellow	H ₂ O	20	10.77	11.79	14.05	16.74	22.06	27.08	33.56	38.65
Quinoline Yellow	EtOH	20	13.51	13.57	13.75	14.41	15.02	15.44	15.92	15.86
Eriochrome Black T	H ₂ O	100	61.75	62.16	63.64	65.60	68.33	70.81	73.07	74.49
Trypan Blue	H ₂ O	100	76.90 ± 2.97	77.77 ± 3.06	80.30 ± 3.32	83.04 ± 3.80	87.08 ± 3.32	90.09 ± 3.05	93.13 ± 2.45	95.61 ± 1.92

mol and Trypan Blue (TB)—872.9 g/mol. The adsorption and photocatalytic degradation efficiency of those dyes onto the tested material are presented in Table 3. The results showed that the lowest efficiency in the sorption process was demonstrated by MB at the level of 13.23%. Both EBT and TB achieved high sorption efficiency at 61.75% and 76.90%, respectively. In each case, the degree of dye removal increased after UV light; however, the largest difference between sorption and photodegradation process was obtained for MB and reached 49,79%. The highest total degradation efficiency was obtained for TB (95,61%). The increase in efficiency for EBT was at around 13%. The reason for this may be the fact that EBT could have been adsorbed at less favourable spots for photocatalytic decomposition than MB and TB.

The fit between the pore size and the molecule size of the substance to be adsorbed has a great impact on the sorption process, which is strongly related to the photocatalytic activity of the material. Small molecules are more likely to adsorb on the microporous surface, while macromolecules easily diffuse into the macro pores. Lu et al. confirmed this dependency by studying the effect of the molecular size of two antibiotics on sorption process onto porous resins. The sorption efficiency of the antibiotics was related to the pore size of the resin. The results showed that Tylosin (TYL), with the molar mass of 916.1 g/mol, reached adsorption effectiveness onto macroporous resin XAD-4 with approximately 110 mg/g, while the amount adsorbed on microporous resin MN-202 was less than 60 mg/g. The results of adsorption of the second of the tested antibiotics—Ciprofloxacin (CIP) with a molar mass of 331.4 g/mol, were opposite. The amount adsorbed on the macroporous resin XAD-4 was about 65 mg/g, whereas for the microporous surface of MN-202 the amount was about 105 mg/g (Lu et al. 2014).

Effect of solvent

Table 4 presents a comparison of the photodegradation efficiency of MB and QY dissolved in water and in ethanol. The sorption efficiency was similar for both dyes and solvents (10–13%), but after the photocatalysis process the efficiency values differed significantly (MB—24.30% and 63.02% for QY—15.86% and 38.65% for EtOH and H₂O, respectively). The use of organic solvent resulted in a lower dye removal rate compared to samples dissolved in water. This effect could be related to the scavenging of OH radicals by organic solvents. The reduction of solvation of excited electrons in organic solvents, in comparison with aqueous solutions, could also have an impact on the photodegradation rate. Therefore, it can be concluded that the more polar solvents should allow a higher degree of degradation to be achieved. The results were consistent by Epling and Lin, who investigated the effect of acetonitrile



concentration in water solution on the photodegradation efficiency of MB. Photodegradation of the dye decreased in the presence of acetonitrile and the degradation rate continued to decrease with increasing acetonitrile concentration. In pure acetonitrile photodegradation was almost undetectable (Epling and Lin 2002). Aarathi et al. studied the effect of mixed MeOH-EtOH solvent systems on photocatalytic degradation of Sudan III. With increasing concentration of ethanol in a mixed system, the photodegradation rate decreased (Aarathi et al. 2007).

Kinetic studies, effect of time investigations on photocatalytic performance

Kinetic studies were carried out for 60 min. The photocatalytic rate constants with determination coefficients for each of the dye solutions were studied and are presented in Table 5. Determination coefficients, as well as rate constant values for processes carried out in ethanol solutions, were lower in comparison with water-solvent processes. A change of solvent from water to ethanol decreased photodegradation more than 10 times. The highest photocatalytic activity was revealed for Trypan Blue with constant rate 0.032 min^{-1} . For an aqueous solution of Methylene Blue, the photocatalytic constant rate ($k = 0.01475 \text{ min}^{-1}$) confirmed good photodegradation of the dye. It could be explained by the low adsorption of Methylene Blue, and a low concentration of the dye onto surface of the photocatalyst. Verma et al. investigated photodegradation of Trypan Blue onto ZnO-ammonia modified graphene oxide. In this conditions, rate constant of Trypan Blue was $7.3 \cdot 10^{-3} \text{ min}^{-1}$ and it was more than seven times higher than for pure ZnO (Verma and Dutta 2017; Wang et al. 2018).

Photocatalyst mechanism

The efficiency of photodegradation processes was influenced by factors associated with the catalyst, degraded material and reaction environment. The addition of iron oxide, in particular Fe_2O_3 , leads to a change in energy levels between the conduction (CB) and valence (VB) bands in the composite. The difference in energy levels between Fe_2O_3 and ZnO leads to the generation of electron that was transferred from the surface of ZnO to Fe_2O_3 . The potential difference between the CB electrons or the VB holes of two semiconductors was the driving force behind electron migration. The transfer of photoproduced electrons from CB ZnO to CB Fe_2O_3 and the holes from VB ZnO to VB Fe_2O_3 were thermodynamically favourable (Karunakaran and Vinayagamoorthy 2017). Recombination of photogenerated electrons and holes was effectively reduced, which extended the life of the material and increased its photocatalytic performance (Li et al. 2017).

On the basis of the analysis of the reaction environment, the significance of the occurrence of hydroxyl groups in aquatic solution was confirmed. The presence of hydroxyl groups was necessary for the transfer of electrons in the photodegradation process and their absence inhibited the decomposition of dyes in UV light. The electron-hole pairs forming on the photocatalyst reacted with water, generating hydroxyl and superoxide radicals necessary to degrade dyes (Jiamprasertboon et al. 2019). Additionally, the properties of the decomposed compounds, such as the charge and size of the substance, had a significant impact on the photocatalytic performance. The charge of dissolved compounds affected in the first stage the process of sorption on the surface of the photocatalyst. The presence of pores of different sizes made it possible to adsorb both small-sized particles (Methylene Blue) and those with complex structures (Trypan Blue), so

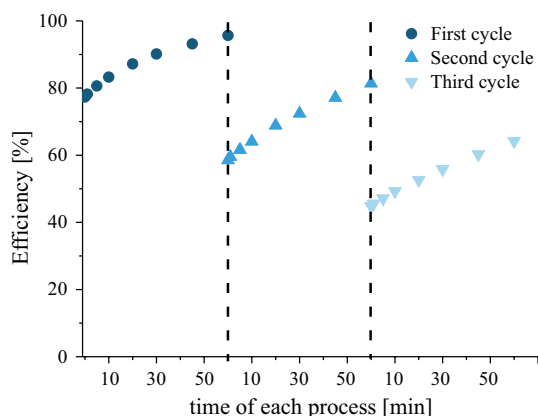
Table 5 Langmuir–Hinshelwood kinetic equations with parameters for photodegradation of dye solutions onto $\text{Fe}_3\text{O}_4/\text{ZnO}$ NPs

Lp.	Dye	Solvent	Equation	k [min^{-1}]	Determination coefficient
1	Methylene Blue	H_2O	$\ln\left(\frac{c}{c_0}\right) = 0.014751 \cdot t - 0.003652$	$14.75 \cdot 10^{-3}$	$R^2 = 0.9961$
2	Methylene Blue	EtOH	$\ln\left(\frac{c}{c_0}\right) = 0.001344 \cdot t - 0.053981$	$1.344 \cdot 10^{-3}$	$R^2 = 0.3021$
3	Methyl Orange	H_2O	$\ln\left(\frac{c}{c_0}\right) = 0.000945 \cdot t - 0.002884$	$0.945 \cdot 10^{-3}$	$R^2 = 0.9869$
4	Quinoline Yellow	H_2O	$\ln\left(\frac{c}{c_0}\right) = 0.006289 \cdot t - 0.006149$	$6.289 \cdot 10^{-3}$	$R^2 = 0.9985$
5	Quinoline Yellow	EtOH	$\ln\left(\frac{c}{c_0}\right) = 0.000508 \cdot t - 0.002900$	$0.508 \cdot 10^{-3}$	$R^2 = 0.8889$
6	Eriochrome Black	H_2O	$\ln\left(\frac{c}{c_0}\right) = 0.006993 \cdot t - 0.023408$	$6.993 \cdot 10^{-3}$	$R^2 = 0.9720$
7	Trypan Blue	H_2O	$\ln\left(\frac{c}{c_0}\right) = 0.031999 \cdot t - 0.064893$	$32.00 \cdot 10^{-3}$	$R^2 = 0.9891$



Table 6 Efficiency of photodegradation of Trypan Blue on the reused $\text{Fe}_3\text{O}_4/\text{ZnO}$ NPs (Zn–Fe-8) during three cycles

Cycle	C_0 (mg/dm ³)	30 min sorption (%)	Photodegradation (after 30 min in the darkness) [%]						
			1 min	5 min	10 min	20 min	30 min	45 min	60 min
I Cycle	100	76.90 ± 2.97	77.77 ± 3.06	80.30 ± 3.32	83.04 ± 3.80	87.08 ± 3.32	90.09 ± 3.05	93.13 ± 2.45	95.61 ± 1.92
II Cycle	100	58.48 ± 0.08	59.48 ± 0.48	61.39 ± 0.33	63.89 ± 0.27	68.20 ± 0.92	71.99 ± 0.57	76.86 ± 0.38	81.22 ± 0.23
III Cycle	100	44.80 ± 1.04	45.55 ± 0.53	47.11 ± 0.88	49.25 ± 1.11	52.61 ± 0.42	55.83 ± 0.38	60.25 ± 0.34	64.23 ± 0.77

**Fig. 8** Efficiency of photodegradation of Trypan Blue on the $\text{Fe}_3\text{O}_4/\text{ZnO}$ NPs (Zn–Fe-8) in subsequent cycles

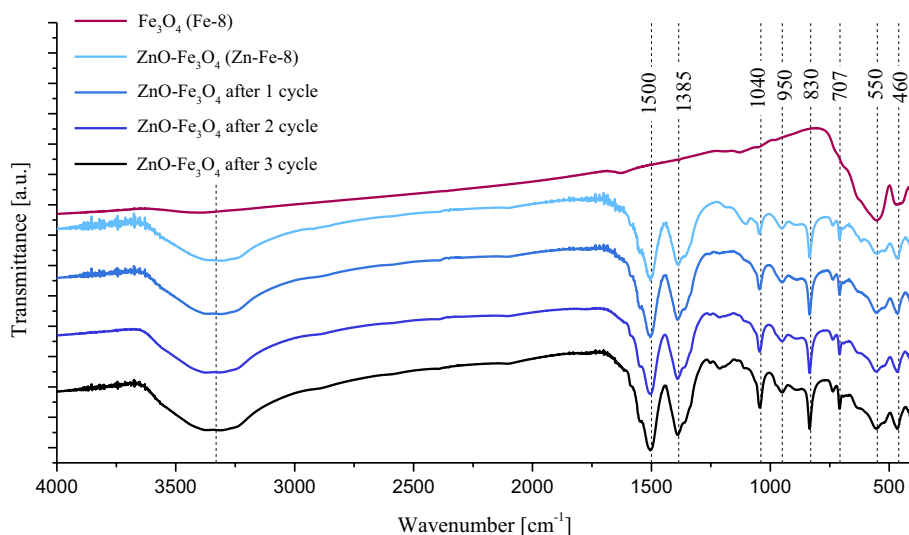
that photodegradation processes could be carried out in subsequent stages. In order to fully understand the mechanism of the process, extensive research is needed using more compounds that are degraded at certain parameters.

Efficiency of dye photodegradation in subsequent cycles

In order to verify the reuse possibility of the catalyst, three cycles of photodegradation of the Trypan Blue were carried out (Table 6 and Fig. 8).

The photocatalytic activity of the $\text{Fe}_3\text{O}_4/\text{ZnO}$ NPs decreased with the increasing number of cycles. The efficiency of the photodegradation of Trypan Blue changed from 95.61 to 64.23% (Fig. 8). The decrease in photocatalytic activity can be the result of two phenomena. First of all, the sorption efficiency decreased rapidly from 77 to 44% and less dye was removed from the solution. Due to less dye adsorption, the efficiency of the photodegradation process also decreased. The relatively complex dye structure and short time of subsequent processes affected the dye content on the nanomaterial after photodegradation. The residual amounts of the adsorbed dye determine the different starting point of the process and thus affect the overall efficiency of the next cycles.

After each cycle, $\text{Fe}_3\text{O}_4/\text{ZnO}$ NPs were analysed with FTIR method to determine structural changes in material (Fig. 9). No significant differences between the photocatalyst before and after photodegradation were observed. After subsequent cycles, an increase in bands at the wave number 1580, 1500, 1040, 950 cm^{-1} was observed, which indicated

Fig. 9 FTIR analysis of Fe_3O_4 (Fe-8), NPs of pure and reused $\text{Fe}_3\text{O}_4/\text{ZnO}$ (Zn–Fe-8)

increasing dye sorption on the material. In addition, the presence of two bands around 2360 and 1210 cm^{-1} were observed, which are characteristic of Trypan Blue (Eskizeybek et al. 2012; Lade et al. 2015).

Conclusion

$\text{Fe}_3\text{O}_4/\text{ZnO}$ NPs were obtained combining the photocatalytic properties of ZnO with the magnetic properties of iron oxides. The photocatalytic material was obtained in a microwave reactor in a two-step precipitation process. In the first step, the Fe_3O_4 was obtained and in the second step ZnO on iron oxides was deposited. XRD analysis and magnetic hysteresis studies have confirmed that, depending on the mass share of $\text{Fe}_2\text{O}_3:\text{FeO}:\text{ZnO}$, materials with variable magnetic and photocatalytic properties were synthesized. The increased share of $\text{Fe}_2\text{O}_3:\text{FeO}$ improved the photocatalytic properties of ZnO. This may be due to the porous structure of Fe_2O_3 , which enhanced the sorption efficiency and consequently affected the photocatalysis efficiency. The presence of the magnetite phase significantly influenced magnetic properties of the material, and thus the possibility of the composite recovery after the photodegradation processes. The proper ratio of all of the three components determined the high effectiveness of dyes removal and easy recovery of material from the mixture using a magnet.

The $\text{Fe}_3\text{O}_4/\text{ZnO}$ material was used in photodegradation studies on a group of dye solutions differing in molar mass, dye charge and solvent. The presence of meso- and macropores in the material allowed for effective sorption of Trypan Blue ($E = 76.9\%$), which in the next stage, enhanced the possibility of the dye-photocatalyst interaction and photodegradation of dyes. It has been confirmed that depending on the type of dye, reaction environment and material structure, the photocatalytic efficiency may reach different values. Possibility of reuse of the photocatalyst was also investigated and confirmed.

Acknowledgements This research did not receive any specific grant from funding agencies in the public, commercial, or not-for-profit sector.

Compliance with ethical standards

Conflict of interest The authors report no declarations of interest.

Open Access This article is licensed under a Creative Commons Attribution 4.0 International License, which permits use, sharing, adaptation, distribution and reproduction in any medium or format, as long as you give appropriate credit to the original author(s) and the source, provide a link to the Creative Commons licence, and indicate if changes were made. The images or other third party material in this article are included in the article's Creative Commons licence, unless indicated

otherwise in a credit line to the material. If material is not included in the article's Creative Commons licence and your intended use is not permitted by statutory regulation or exceeds the permitted use, you will need to obtain permission directly from the copyright holder. To view a copy of this licence, visit <http://creativecommons.org/licenses/by/4.0/>.

References

- Aarthi T, Narahari P, Madras G (2007) Photocatalytic degradation of Azure and Sudan dyes using nano TiO_2 . *J Hazard Mater* 149:725–734. <https://doi.org/10.1016/j.jhazmat.2007.04.038>
- Abbas N, Shao GN, Haider MS et al (2016) Sol–gel synthesis of $\text{TiO}_2\text{-Fe}_2\text{O}_3$ systems: effects of Fe_2O_3 content and their photocatalytic properties. *J Ind Eng Chem* 39:112–120. <https://doi.org/10.1016/j.jiec.2016.05.015>
- Abdel-Wahab MS, Jilani A, Yahia IS, Al-Ghamdi AA (2016) Enhanced the photocatalytic activity of Ni-doped ZnO thin films: morphological, optical and XPS analysis. *Superlattices Microstruct* 94:108–118. <https://doi.org/10.1016/j.spmi.2016.03.043>
- Ahn MS, Ahmad R, Bhat KS et al (2018) Fabrication of a solution-gated transistor based on valinomycin modified iron oxide nanoparticles decorated zinc oxide nanorods for potassium detection. *J Colloid Interface Sci* 518:277–283. <https://doi.org/10.1016/j.jcis.2018.02.041>
- Aliahmad M, Nasiri Moghaddam N (2013) Synthesis of maghemite ($\gamma\text{-Fe}_2\text{O}_3$) nanoparticles by thermal-decomposition of magnetite (Fe_3O_4) nanoparticles. *Mater Sci Pol* 31:264–268. <https://doi.org/10.2478/s13536-012-0100-6>
- Alqadami AA, Naushad M, Abdalla MA et al (2017) Efficient removal of toxic metal ions from wastewater using a recyclable nanocomposite: a study of adsorption parameters and interaction mechanism. *J Clean Prod* 156:426–436. <https://doi.org/10.1016/j.jclepro.2017.04.085>
- Andrade MB, Guerra ACS, Santos TRT et al (2019) Innovative adsorbent based on graphene oxide decorated with $\text{Fe}_2\text{O}_3/\text{ZnO}$ nanoparticles for removal of dipyrone from aqueous medium. *Mater Lett* 238:233–236. <https://doi.org/10.1016/j.matlet.2018.11.168>
- Atla SB, Lin WR, Chien TC et al (2018) Fabrication of $\text{Fe}_3\text{O}_4/\text{ZnO}$ magnetite core shell and its application in photocatalysis using sunlight. *Mater Chem Phys* 216:380–386. <https://doi.org/10.1016/j.matchemphys.2018.06.020>
- Bel Hadjiltaief H, Ben Ameer S, Da Costa P et al (2018) Photocatalytic decolorization of cationic and anionic dyes over ZnO nanoparticle immobilized on natural Tunisian clay. *Appl Clay Sci* 152:148–157. <https://doi.org/10.1016/j.clay.2017.11.008>
- Ben Arfi R, Karoui S, Mougine K, Ghorbal A (2017) Adsorptive removal of cationic and anionic dyes from aqueous solution by utilizing almond shell as bioadsorbent. *Euro-Mediterr J Environ Integr* 2:20. <https://doi.org/10.1007/s41207-017-0032-y>
- Bertolucci E, Galletti AMR, Antonetti C, et al (2015) Chemical and magnetic properties characterization of magnetic nanoparticles. *Conf Rec IEEE Instrum Meas Technol Conf* 2015 1492–1496. <https://doi.org/10.1109/I2MTC.2015.7151498>
- Dehghan S, Jafari AJ, Farzadkia M et al (2019) Visible-light-driven photocatalytic degradation of Metalaxyl by reduced graphene oxide/ $\text{Fe}_3\text{O}_4/\text{ZnO}$ ternary nanohybrid: influential factors, mechanism and toxicity bioassay. *J Photochem Photobiol A Chem* 375:280–292. <https://doi.org/10.1016/j.jphotochem.2019.01.024>
- Elazab HA, Moussa S, Brinkley KW et al (2017) The continuous synthesis of Pd supported on Fe_3O_4 nanoparticles: a highly effective and magnetic catalyst for CO oxidation. *Green Process Synth* 6:413–424. <https://doi.org/10.1515/gps-2016-0168>



- Elilarassi R, Chandrasekaran G (2017) Optical, electrical and ferromagnetic studies of ZnO: Fe diluted magnetic semiconductor nanoparticles for spintronic applications. *Spectrochim Acta Part A Mol Biomol Spectrosc* 186:120–131. <https://doi.org/10.1016/J.SAA.2017.05.065>
- Epling GA, Lin C (2002) Investigation of retardation effects on the titanium dioxide photodegradation system. *Chemosphere* 46:937–944. [https://doi.org/10.1016/S0045-6535\(01\)00172-2](https://doi.org/10.1016/S0045-6535(01)00172-2)
- Eskizeybek V, Sari F, Gülce H et al (2012) Preparation of the new polyaniline/ZnO nanocomposite and its photocatalytic activity for degradation of methylene blue and malachite green dyes under UV and natural sun lights irradiations. *Appl Catal B Environ* 119–120:197–206. <https://doi.org/10.1016/j.apcatb.2012.02.034>
- Fernández L, Gamallo M, González-Gómez MA et al (2019) Insight into antibiotics removal: exploring the photocatalytic performance of a Fe₃O₄/ZnO nanocomposite in a novel magnetic sequential batch reactor. *J Environ Manage* 237:595–608. <https://doi.org/10.1016/j.jenvman.2019.02.089>
- Fowsiya J, Madhumitha G, Al-Dhabi NA, Arasu MV (2016) Photocatalytic degradation of Congo red using *Carissa edulis* extract capped zinc oxide nanoparticles. *J Photochem Photobiol B Biol* 162:395–401. <https://doi.org/10.1016/J.JPHOTOBIOL.2016.07.011>
- Garino N, Limongi T, Dumontel B et al (2019) A microwave-assisted synthesis of zinc oxide nanocrystals finely tuned for biological applications. *Nanomaterials* 9:1–17. <https://doi.org/10.3390/nano9020212>
- Ghosh M, Manoli K, Shen X et al (2019) Solar photocatalytic degradation of caffeine with titanium dioxide and zinc oxide nanoparticles. *J Photochem Photobiol A Chem* 377:1–7. <https://doi.org/10.1016/J.JPHOTOCHEM.2019.03.029>
- Goyal P, Chakraborty S, Misra SK (2018) Multifunctional Fe₃O₄-ZnO nanocomposites for environmental remediation applications. *Environ Nanotechnology, Monit Manag* 10:28–35. <https://doi.org/10.1016/j.enmm.2018.03.003>
- Güy N, Atacan K, Karaca E, Özacar M (2018) Role of Ag₃PO₄ and Fe₃O₄ on the photocatalytic performance of magnetic Ag₃PO₄/ZnO/Fe₃O₄ nanocomposite under visible light irradiation. *Sol Energy* 166:308–316. <https://doi.org/10.1016/j.solener.2018.03.045>
- Han R, Li W, Pan W et al (2014) 1D magnetic materials of Fe₃O₄ and Fe with high performance of microwave absorption fabricated by electrospinning method. *Sci Rep* 4:1–5. <https://doi.org/10.1038/srep07493>
- Hernández A, Maya L, Sánchez-Mora E, Sánchez EM (2007) Sol-gel synthesis, characterization and photocatalytic activity of mixed oxide ZnO-Fe₂O₃. *J Sol-Gel Sci Technol* 42:71–78. <https://doi.org/10.1007/s10971-006-1521-7>
- Jiamprasertboon A, Kafizas A, Sachs M, Ling M, Alotaibi AM, Lu Y, Siritanon T, Parkin IP, Carmalt CJ (2019) Heterojunction α -Fe₂O₃/ZnO films with enhanced photocatalytic properties grown by aerosol-assisted chemical vapour deposition. *Chem Euro J* 25(48):11337–11345
- Kansal SK, Singh M, Sud D (2007) Studies on photodegradation of two commercial dyes in aqueous phase using different photocatalysts. *J Hazard Mater* 141:581–590. <https://doi.org/10.1016/J.JHAZMAT.2006.07.035>
- Kant S, Kumar A (2012) A comparative analysis of structural, optical and photocatalytic properties of ZnO and Ni doped ZnO nanoparticles prepared by sol-gel method. *Adv Mater Lett* 3:350–354. <https://doi.org/10.5185/amlett.2012.5344>
- Kucharczyk K, Rybka JD, Hilgendorff M et al (2019) Composite spheres made of bioengineered spider silk and iron oxide nanoparticles for theranostics applications. *PLoS ONE* 14:e0219790. <https://doi.org/10.1371/journal.pone.0219790>
- Lade H, Kadam A, Paul D, Govindwar S (2015) A low-cost wheat bran medium for biodegradation of the benzidine-based carcinogenic dye Trypan Blue using a microbial consortium. *Int J Environ Res Public Health* 12:3480–3505. <https://doi.org/10.3390/ijerph120403480>
- Lee KM, Abd Hamid SB, Lai CW (2015) Mechanism and kinetics study for photocatalytic oxidation degradation: a case study for phenoxyacetic acid organic pollutant. *J Nanomater* 2015:1–10. <https://doi.org/10.1155/2015/940857>
- Li N, Zhang J, Tian Y, Zhao J, Zhang J, Zuo W (2017) Precisely controlled fabrication of magnetic 3D γ -Fe₂O₃@ZnO core-shell photocatalyst with enhanced activity: Ciprofloxacin degradation and mechanism insight. *Chem Eng J* 308:377–385
- Lu Y, Jiang M, Wang C et al (2014) Impact of molecular size on two antibiotics adsorption by porous resins. *J Taiwan Inst Chem Eng* 45:955–961. <https://doi.org/10.1016/j.tjce.2013.09.009>
- Mieloch AA, Kręcis M, Rybka JD et al (2018) The influence of ligand charge and length on the assembly of Brome mosaic virus derived virus-like particles with magnetic core. *AIP Adv*. <https://doi.org/10.1063/1.5011138>
- Morales AE, Mora ES, Pal U (2007) Use of diffuse reflectance spectroscopy for optical characterization of un-supported nanostructures. *Rev Mex Fis* 53:18–22
- Naqvi SMA, Soleimani H, Yahya N, Irshad K (2014) Structural and optical properties of chromium doped zinc oxide nanoparticles synthesized by sol-gel method. *1621:530–537*. <https://doi.org/10.1063/1.4898517>
- Patil SP, Bethi B, Sonawane GH et al (2016) Efficient adsorption and photocatalytic degradation of Rhodamine B dye over Bi₂O₃-bentonite nanocomposites: a kinetic study. *J Ind Eng Chem* 34:356–363. <https://doi.org/10.1016/J.JIEC.2015.12.002>
- Regulacio MD, Han M-Y (2016) Multinary I–III–VI₂ and I₂–II–IV–VI₄ Semiconductor Nanostructures for Photocatalytic Applications. *Acc Chem Res* 49:511–519. <https://doi.org/10.1021/acs.accounts.5b00535>
- Riyadh MA, Quraish AK, Kassim MS et al (2015) Synthesis of zinc oxide nanoparticles via sol-gel route and their characterization. *J Environ Manage* 5:1–6. <https://doi.org/10.5923/j.nm.20150501.01>
- Rodrigues CSD, Soares OSGP, Pinho MT et al (2017) p-Nitrophenol degradation by heterogeneous Fenton's oxidation over activated carbon-based catalysts. *Appl Catal B Environ* 219:109–122. <https://doi.org/10.1016/j.apcatb.2017.07.045>
- Sin JC, Tan SQ, Quek JA et al (2018) Facile fabrication of hierarchical porous ZnO/Fe₃O₄ composites with enhanced magnetic, photocatalytic and antibacterial properties. *Mater Lett* 228:207–211. <https://doi.org/10.1016/j.matlet.2018.06.027>
- Türkyılmaz ŞŞ, Güy N, Özacar M (2017) Photocatalytic efficiencies of Ni, Mn, Fe and Ag doped ZnO nanostructures synthesized by hydrothermal method: the synergistic/antagonistic effect between ZnO and metals. *J Photochem Photobiol A Chem* 341:39–50. <https://doi.org/10.1016/j.jphotochem.2017.03.027>
- Verma S, Dutta RK (2017) Enhanced ROS generation by ZnO-ammonia modified graphene oxide nanocomposites for photocatalytic degradation of trypan blue dye and 4-nitrophenol. *J Environ Chem Eng* 5:4776–4787. <https://doi.org/10.1016/J.JECE.2017.08.026>
- Wang J, Yang J, Li X et al (2016) Preparation and photocatalytic properties of magnetically reusable Fe₃O₄@ZnO core/shell nanoparticles. *Phys E Low-Dimensional Syst Nanostruct* 75:66–71. <https://doi.org/10.1016/j.physe.2015.08.040>
- Wang H, Zhou P, Guo R et al (2018) Synthesis of rectorite/Fe₃O₄/ZnO composites and their application for the removal of methylene blue dye. *Catalysts*. <https://doi.org/10.3390/catal8030107>
- Wierzbinski KR, Szymanski T, Rozwadowska N et al (2018) Potential use of superparamagnetic iron oxide nanoparticles for in vitro and in vivo bioimaging of human myoblasts. *Sci Rep*. <https://doi.org/10.1038/s41598-018-22018-0>

